IEICE TRANS. FUNDAMENTALS, VOL. E81-A, NO. 7 JULY 1998

PAPER Special Section on Fundamentals of Multi-dimensional Mobile Information Network

# Proposal of Chirp Multiplexing Transform/Intensity Modulation/Direct Detection System for Radio Highway Networks

Yozo SHOJI†, Katsutoshi TSUKAMOTO†, *and* Shozo KOMAKI†, *Members*

**SUMMARY** This paper newly proposes the CMT/IM/DD system for universal radio access networks where radio base stations (RBSs) and an optic backbone network are universally available among different radio services and providers. In the proposed system, the Chirp Fourier transformer at an RBS, converts the received FDM multiple radio service signals into optical TDM format signals, then transfers them over the optic fiber-link. This paper is focused on the discussion about the performance on the up-link of the CMT/IM/DD system. A new type of the configuration of CMT and the direct demodulation for the CMT signal are also proposed, and the SNR considering inter-symbol and inter-channel interferences caused by the CMT is theoretically analyzed. Analysis results show that the overall SNR performance of the CMT system is superior to the conventional SCM system when the number of radio channels is more than 26.

***key words:*** *chirp multiplexing transform, FDM-to-TDM conversion, routing, radio highway networks, fiber-optic microcellular systems*

## 1. Introduction

Fiber-optic microcellular personal communication systems (PCS's), where a large number of inexpensive radio base stations (RBSs) are connected via optical fiber to a single control station (CS) at an economical location, have many advantages such as flexible deployment, rapid roll-out, high frequency efficiency, cost-effectiveness and reduction of power consumption of handsets. The goals of microcellular PCS's include provision of multiple services such as voice, data, picture, and video. A single optic-fiber link has a great broadband characteristic enough to deliver multiple radio services all together. However different providers tend to independently construct their own infrastructures for reasons of the difference of service, frequency band, and radio signal format. It needs a vast investment of time and cost to construct a new infrastructure.

To solve the problem, we have proposed the concept of Radio Highway Networks [1]–[4] as a new type of radio access networks universally available for any kind of radio signal. The Radio Highway Networks can reduce the time and the cost for new infrastructures, keeping the advantages of microcellular system, since different radio services can share RBSs and a backbone optical network. Different radio services are ordinarily operated by different providers in different frequency bands, and their CSs are located at different places. So in order to handle multiple services universally, the Radio Highway Networks need the routing node (RN) to distinct and switch each service signal into its desired CS.

The conventional link to transfer radio signals via optic-fiber is subcarrier multiplexing/intensity modulation/direct detection (SCM/IM/DD) link, which has the advantages in simplicity and cost-effectiveness of RBSs [5]. However from the viewpoint of the realization of RN, the SCM/IM/DD link has a primary disadvantage that the distinction of the desired service signal at RN cannot be performed until all of the optical signals are photo-detected because the multiple radio services are transfered over optic fiber in electrical FDM format.

To solve this problem, this paper newly proposes the new application of Chirp Fourier transformer (CFT) [6] to the Radio Highway Networks. We describe the applied system as Chirp Multiplexing Transform (CMT)/IM/DD system, where CMT at each RBS converts the multiple service radio signals operated in the different frequency bands into those operated in TDM format before optical transmission. The converted CMT signal can be demodulated by direct demodulator or using Inverse CMT. The benefit of this system is that the extraction of the desired service can be easily performed in optical domain by photonic time switching. About the photonic time switching to date, there are progressing techniques such as self-routing photonic switching [7], and we can expect the fast switch operation, the high cost-efficiency and the large capacity. As the alternative to CFT, you may think of the FDM-to-TDM conversion scheme using digital signal processing [8]. However it isn't suitable for our purpose because it spoils the flexibility of RBSs due to the requirement of digital processing and cannot handle very broadband radio signals. On the other hand, the CFT realized by SAW (surface acoustic wave) devices is suitable because of its broadband characteristics and the function as a real-time analog Fourier transformer.

The CFT has been studied in many applications

Manuscript received November 17, 1997.
Manuscript revised February 17, 1998.

† The authors are with the Faculty of Engineering, Osaka university, Suita-shi, 565–0871 Japan.

such as spectrum analyzer[6], time compression of signal[9], and multiplexer and demultiplexer in satellite communications[10]. Especially group demodulator using the CFT is proposed in [11],[12] where FDM radio signals are transformed into TDM signal by the CFT and demodulated by digital processing. And the bit error rate performance is clarified by using simulation analysis. However there has been no study of signal performance in the CMT/IM/DD system where CFT signals are transfered via optic-fiber link. Therefore this paper proposes a new type of the configuration of CMT/IM/DD system and theoretically analyzes the signal-to-noise power ratio performance on up-link considering the nonlinearity of LD, the receiver noises in optical IM/DD link, and inter-channel interferences (ICI) and inter-symbol interferences (ISI) caused by the CMT. Furthermore this paper shows that the parallel use of CFT proposed in [12] is also effective to improve the signal-to-noise power ratio of the CMT/IM/DD system.

This paper is organized as follows, Sect. 2 describes the principle of CMT. Section 3 clarifies the characteristic of the CMT signal. Section 4 describes the direct demodulation scheme for the CMT signal and theoretically analyzes signal to inter-channel interference power ratio ($S/ICI$) and signal to inter-symbol interference power ratio ($S/ISI$). Next, Sect. 5 proposes a new type of CMT to reduce ICI and ISI. Finally Sect. 6 theoretically analyzes signal to noise power ratio (SNR) taking into account the LD nonlinearity and overall performance including SNR, S/ICI and S/ISI, and compares them with those of the conventional SCM system.

## 2. Principle of Chirp Multiplexing Transform

Figure 1 illustrates the configuration of Radio Highway using a proposed CMT/IM/DD system. It consists of the universal RBSs, CSs for each radio service, an RN, and optic-fiber links to connect them. The universal RBSs are equipped with CMT and E/O converter. As shown in Fig. 1, the CMT converts multiple radio service signals operated in multiband into those operated in TDM format, and the converted signals are transmitted into a optic-fiber link with E/O conversion. An

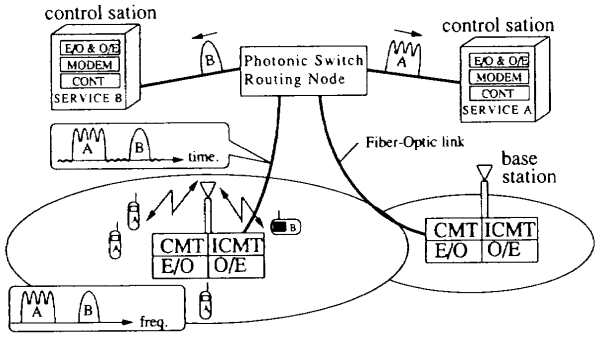


**Fig. 1** Radio high-way networks using CMT/IM/DD system.

RN distinguishes each service by its time position and switches it into the desired CS by use of a simple photonic switch.

To investigate the operation of CMT, we assume the bandlimited signal $r(t)$.

$$r(t) = Re[u(t)e^{j2\pi f_0 t}] \tag{1}$$

where $u(t)$ is the complex envelope whose spectrum is bandlimited into $|f| \leqq \frac{B_{total}}{2}$ and $f_0$ is the center frequency. The configuration of CMT is shown in Fig. 2. The CMT process is twice multiplication with a chirp signal and a filtering with a chirp filter, but two identical processes (upper and lower process in Fig. 2) in parallel with an alternate gating function are needed in order to obtain successive transformed output signals.

The first process in CMT is the pre-multiplication of $r(t)$ with an up-chirp signal, $C_a(t)$. The term "up-chirp" means that its frequency increases as time passes, while "down-chirp" means that its frequency decreases. An up-chirp signal can be obtained as an impulse response of an up-chirp filter in which the higher frequency component is delayed longer. Introducing a complex low-pass up-chirp signal $c(t)$, the up-chirp signal with its center frequency $f_a$, $C_a(t)$, is given by [9]

$$C_a(t) = Re[\sqrt{2}c(t)e^{j2\pi f_a t}] \tag{2}$$

$$c(t) = \begin{cases} \exp(j2\pi\beta t^2/2) & (-\frac{T_c}{2} \leqq t \leqq \frac{T_c}{2}) \\ 0 & (\text{otherwise}) \end{cases} \tag{3}$$

where $\beta$ is the chirp slope in [Hz/s] and $T_c$ is the chirping dispersion time. Then we can define the frequency range of sweep, $\Delta F$, as

$$\Delta F = \beta T_c \tag{4}$$

For the upper and the lower processes, we need two alternately gated up-chirp signals with their period $2T_c$, $C_u(t)$ and $C_l(t)$. They are obtained by multiplying a successive up-chirp signal with its period $T_c$, $\sum_{k=-\infty}^{\infty} C_a(t - kT_c)$, by two alternate gating functions, $G(t)$ and $G(t - T_c)$, with their period $2T_c$:

$$G(t) = \sum_{k=-\infty}^{\infty} g(t - 2kT_c) \tag{5}$$

$$g(t) = \begin{cases} 1 & (-\frac{T_c}{2} \leqq t \leqq \frac{T_c}{2}) \\ 0 & (\text{otherwise}) \end{cases} \tag{6}$$

Then $C_u(t)$ and $C_l(t)$ are written by

$$C_u(t) = \sum_{m=-\infty}^{\infty} C_a(t - 2mT_c) \tag{7}$$

$$C_l(t) = \sum_{m=-\infty}^{\infty} C_a(t - (2m+1)T_c) \tag{8}$$

The radio signal $r(t)$ is multiplied by the gated up-chirp signals, $C_u(t)$ and $C_l(t)$, separately on the upper path and the lower path as shown in Fig. 2. The

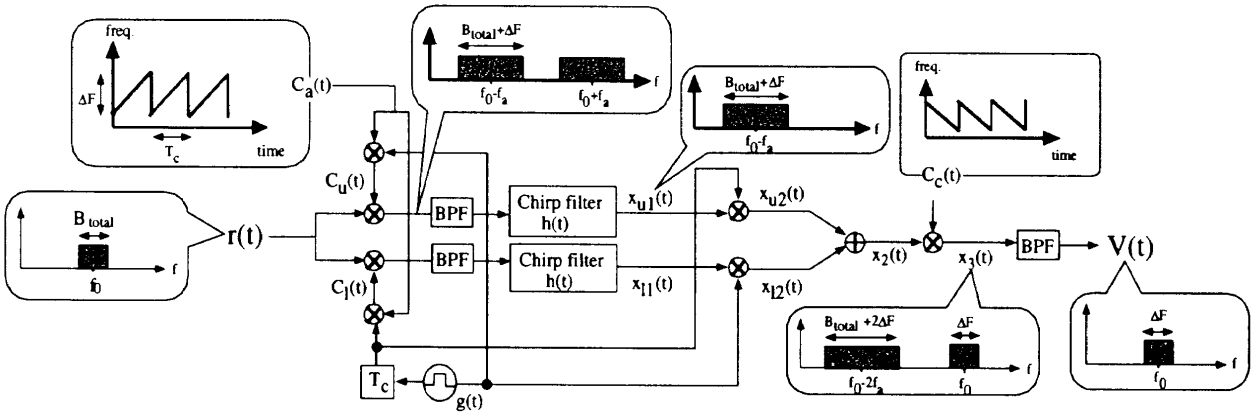


**Fig. 2** Configuration of CMT.

multiplication generates two components in $(f_0 - f_a)$ frequency band and $(f_0 + f_a)$ frequency band. Any image frequency component and any overlap of the two frequency band signals are not generated in the case of $|f_0 - f_a| \gg (\Delta F + B_{total})/2$ and $f_a \gg (\Delta F + B_{total})/2$. Therefore we can use either of frequency band signals for the next filtering process using a down-chirp filter. However since the carrier frequency of radio signal $f_0$ is microwave or millimeter wave band in recent trend, it seems comparatively difficult to realize a chirp filter with high frequency, $(f_0 + f_a)$. Consequently it is reasonable to use the up-chirp filter in the lower frequency band $(f_0 - f_a)$ for the filtering process. Hence,

$$r(t) \cdot C_u(t) = Re\left[\sum_{m=-\infty}^{\infty} \frac{\sqrt{2}}{2} u(t) c^*(t - 2mT_c) e^{j2\pi(f_0 - f_a)t}\right] \quad (9)$$

$$r(t) \cdot C_l(t) = Re\left[\sum_{m=-\infty}^{\infty} \frac{\sqrt{2}}{2} u(t) c^*(t - (2m+1)T_c) e^{j2\pi(f_0 - f_a)t}\right] \quad (10)$$

and the impulse response of the up-chirp filter, $h(t)$, is given by

$$h(t) = \begin{cases} Re\left[\sqrt{\beta} e^{j2\pi(\frac{\beta}{2}t^2 - \Delta F t)} \cdot e^{j2\pi(f_0 - f_a)t}\right] \\ \quad (0 \leqq t \leqq 2T_c) \\ 0 \quad \text{(otherwise)} \end{cases} \quad (11)$$

Therefore, the outputs after the filtering process on each path, $x_{u1}(t)$ and $x_{u2}(t)$ are written by

$$x_{u1}(t) = \{r(t)C_u(t)\} \otimes h(t) = Re\left[\sum_{m=-\infty}^{\infty} U^{(2m)}(t) C_{if}^{(2m)}(t)\right] \quad (12)$$

$$x_{l1}(t) = \{r(t)C_l(t)\} \otimes h(t) = Re\left[\sum_{m=-\infty}^{\infty} U^{(2m+1)}(t) C_{if}^{(2m+1)}(t)\right] \quad (13)$$

where $\otimes$ denotes convolution, and $U^{(k)}(t)$ and $C_{if}^{(k)}(t)$ are given by

$$U^{(k)}(t) = \begin{cases} \int_{-\frac{T_c}{2}}^{t} u(\tau + kT_c) e^{-j2\pi\beta[t-(k+1)T_c]\tau} d\tau \\ \quad (-T_c/2 \leqq t - kT_c < T_c/2) \\ \int_{-\frac{T_c}{2}}^{\frac{T_c}{2}} u(\tau + kT_c) e^{-j2\pi\beta[t-(k+1)T_c]\tau} d\tau \\ \quad (T_c/2 \leqq t - kT_c \leqq 3T_c/2) \\ \int_{t-2T_c}^{\frac{T_c}{2}} u(\tau) e^{-j2\pi\beta[t-T_c]\tau} d\tau \\ \quad (3T_c/2 < t - kT_c \leqq 5T_c/2) \\ 0 \quad \text{(otherwise)} \end{cases} \quad (14)$$

$$C_{if}^{(k)}(t) = \frac{\sqrt{2\beta}}{4} e^{j2\pi\beta\frac{[t-(k+1)T_c]^2}{2}} \cdot e^{j2\pi(f_0 - f_a)t} \quad (15)$$

Figure 3 illustrates the input and the output signals of the chirp filter in the time domain. In Eq. (14), the part in the range of $\frac{T_c}{2} \leqq t - kT_c \leqq \frac{3T_c}{2}$, that is, $U^{(k)}(t)g(t-(k+1)T_c)$ is shown as the shadowed part in Fig. 3. It corresponds to the Fourier transform of $u(t)$ gated in the time range $T_c$ necessary for our purpose. Then, the necessary parts from each path, $x_{u2}(t)$ and $x_{l2}(t)$ are extracted by gating functions, and summed. The result is written by $x_2(t)$.

$$x_2(t) = Re\left[\sum_{k=\infty}^{\infty} U^{(k)}(t) C_{if}^{(k)}(t) g(t - (k+1)T_c)\right] \quad (16)$$

It is found from Eq. (16) that the center frequency of $x_2(t)$ increases periodically due to $C_{if}^{(k)}(t)$. It can be eliminated by further multiplying $x_2(t)$ by a down-chirp signal $C_c(t)$, which is given by

$$C_c(t) = Re[\sqrt{2}c^*(t)e^{j2\pi f_a t}] \quad (17)$$

After band-pass filtering the $x_3(t)$ $(= x_2(t) \cdot C_c(t))$ with its center frequency $f_0$, we finally obtain the desired CMT signal, $V(t)$.

$$V(t) = Re[v(t)e^{j2\pi f_0 t}] \quad (18)$$

$$v(t) = \sum_{k=-\infty}^{\infty} U^{(k)}(t) \cdot g(t - (k+1)T_c) \quad (19)$$

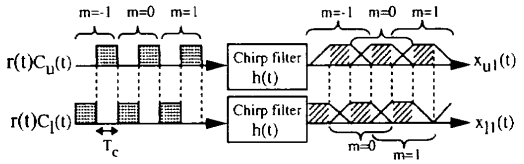


**Fig. 3** Input and output signals of the chirp filter.

where the amplitude constant $\sqrt{2\beta}/8$ and the phase constant are dropped. $U^{(k)}(t)\cdot g(t-(k+1)T_c)$ is referred to as Time Limited Fourier Transform (TLFT) signal in this paper because it is the Fourier transform output of $u(t+kT_c)\cdot g(t)$ where the conversion of the frequency axis to the time axis, that is, $f$ axis to $\beta t$ axis is executed. The time waveform of the TLFT signal represents the spectrum information of $u(t+kT_c)\cdot g(t)$, but it is further limited in the time range of $T_c$. Consequently it is necessary that $\beta T_c$ covers the spectrum range of radio signals, $B_{total}$.

$$\Delta F = \beta T_c \geqq B_{total} \tag{20}$$

Under this condition, the CMT can successfully perform FDM-to-TDM conversion of radio signals. On the other hand, we supplement that the spectrum shape of the TLFT signal represents the time waveform of $u(t+kT_c)\cdot g(t)$, and also bandlimited in the range of $\beta T_c = \Delta F$.

## 3. Consideration on CMT/IM/DD System for FDM-PSK Signals

In this section, we discuss the characteristics of the CMT signal assuming FDM-PSK radio signals. Figure 4 shows the analysis models of CMT/IM/DD system and SCM/IM/DD system for a compared system. In the CMT/IM/DD system, the CMT signal whose low-pass equivalent is represented by Eq. (19) directly modulates Laser Diode (LD) and is transfered via optic-link. The receiver at the CS detects the optic signal and directly demodulates the information using the proposed demodulator described in Sect. 4. On the other hand, in the SCM system, the FDM-PSK signal directly modulates LD and is similarly transfered via optic-link and the information is demodulated by optimum demodulation using matched filter at the CS.

The low-pass equivalent of FDM-PSK radio signals with $(2M+1)$ channels is written by

$$u(t) = \sum_{l=-M}^{M}\sum_{n=-\infty}^{\infty} f(t-nT)e^{j[2\pi l\Delta f t+\theta_{ln}]} \tag{21}$$

where $\theta_{ln}$ is the $n$-th modulation phase of the $l$-th FDM channel. $T$, $\Delta f$, and $f(t)$ are the symbol duration, the channel separation, and the pulse waveform bandlimited into $B$, respectively. Then the total bandwidth, $B_{total}$, is written by

$$B_{total} = (2M+1)\Delta f \tag{22}$$

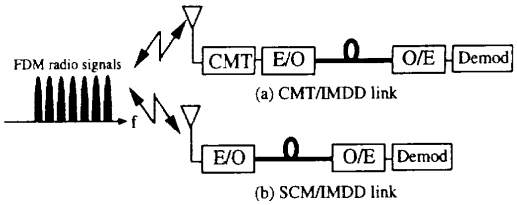


**Fig. 4** Performance analysis models of CMT/IM/DD system and SCM system.

We investigate the $k=0$th TLFT signal in $v(t)$ when Eq. (21) is substituted into Eq. (19). We represent it as $v_0(t)$.

$$v_0(t) = \int_{-\frac{T_c}{2}}^{\frac{T_c}{2}} u(\tau)e^{-j2\pi\beta(t-T_c)\tau}d\tau \left(\frac{T_c}{2} \leqq t \leqq \frac{3}{2}T_c\right) \tag{23}$$

Assuming the perfect synchronization between the symbol timing of $u(t)$ and the chirping dispersion time $T_c$, $v_0(t)$ becomes

$$v_0(t) = \sum_{l=-M}^{M}\sum_{n=-\infty}^{\infty} S_{ln}(t)\cdot e^{j\theta_{ln}} \left(\frac{T_c}{2} \leqq t \leqq \frac{3}{2}T_c\right) \tag{24}$$

$$S_{ln}(t) = \beta G(\beta t) \otimes \left[F[\beta(t-T_c)-l\Delta f]e^{-j2\pi[\beta(t-T_c)-l\Delta f]nT}\right] \tag{25}$$

where $G(f)$ and $F(f)$ are the Fourier transforms of $g(t)$ and $f(t)$ respectively. $S_{ln}(t)$ corresponds to the pulse waveform of the $n$-th symbol of the $l$-th channel. Note that the words "channel" and "symbol number" described in this paper consistently indicate those in the original FDM-PSK radio signals defined in Eq. (21).

Equations (24) and (25) can be generally applied to any kind of pulse waveform, $f(t)$, and any value of $\Delta f$. However we focus our discussion on the case that $f(t)$ is pulse-shaped by the root Nyquist filter. Then $F(f)$ is given by [13]

$$F(f)=\begin{cases} 1 & (0 \leq |f| \leq \frac{1-\alpha}{2T}) \\ \cos\left[\frac{\pi T}{2\alpha}\left(|f|-\frac{1-\alpha}{2T}\right)\right] & \left(\frac{1-\alpha}{2T} < |f| \leq \frac{1+\alpha}{2T}\right) \\ 0 & (\text{otherwise}) \end{cases} \tag{26}$$

where $\alpha$ is the roll-off index. Figure 5 illustrates the relationship between the original radio signal $u(t)$ and its spectrum $U(f)$ and the resultant CMT signal $v_0(t)$ and its spectrum $V_0(f)$. It is seen from Eq. (25) and Fig. 5 that the CMT signal consists of multicarrier PSK signals with carrier spacing $\beta T$, and pulse duration $\Delta f/\beta$. The different symbol in a certain channel is converted to the different carrier frequency in the same time slot, while the different channel's symbol is converted to the different time slot. Furthermore, the CMT signal is rectangularly bandlimited into the frequency range of $\Delta F$,

and its time waveform is limited into the time range of $T_c$, as described in Sect. 2.

If the chirping dispersion time, $T_c$, is infinite ($T_c \to \infty$), we can ignore the convolution with $G(\beta t)$ in Eq. (25), thereby the set of $S_{ln}(t)(l = -M, \cdots, M; n = -\infty, \cdots, \infty)$ becomes orthogonal set and no ICI and no ISI occur (see Appendix). However it can be seen from Eq. (25) and Fig. 5 that in the resultant time domain, each pulse waveform corresponding to a channel, $F(\beta t - l\Delta f) \otimes G(\beta t)$, has a spreading sidelobe even if $F(f)$ is perfectly bandlimited. This spread causes interchannel interference (ICI). On the other hand, in the resultant frequency domain, each spectrum shape corresponding to a symbol, $f(f/\beta - nT) \cdot g(f/\beta)$, is partially truncated. This truncation causes intersymbol interferences (ISI) because of the imperfection of the orthogonality between different symbols even if the set of $f(t - nT)(n = -\infty, \cdots, \infty)$ is orthogonal set.

Here in order to estimate the number of carriers to be considered in the following analysis, we examine the symbol energy of $S_{ln}(t)$. Figure 6 shows the symbol energy of $S_{0n}$ normalized by the symbol energy of $S_{00}$ versus the symbol number $n$ in the case of $T_c/T = 5.0$. It is seen that the energy of the symbols out of center $T_c/T$ symbols, that is, the energy of $S_{0-3}$ and $S_{03}$ in this example, suddenly decreases, and it is less than $-36$ [dB] of the energy of $S_{00}$ at $\alpha = 1.0$. Consequently, we approximate the number of carriers considered in the following discussion as $T_c/T$. Then when $T_c/T$ is represented by $(2p+1$;p is a positive integer), $v_0(t)$ can be rewritten as

$$v_0(t) \approx \sum_{l=-M}^{M} \sum_{n=-p}^{p} S_{ln}(t) e^{j\theta_{ln}} \tag{27}$$

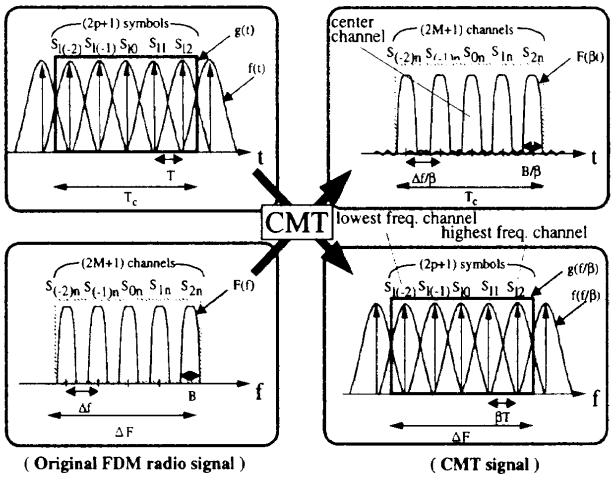


**Fig. 5** Radio signal and CMT signal.

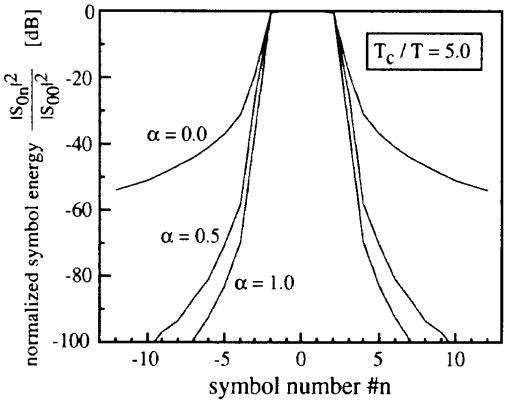


**Fig. 6** Normalized symbol energy versus symbol number.

## 4. ICI and ISI Performance Analysis

Figure 7 shows the configuration of the proposed suboptimal correlation receiver. The term "suboptimal" indicates that the correlated waveform with the received CMT signal in the receiver is the waveform neglecting the convolution with $G(\beta t)$ in Eq. (25). The demodulator performs the multiplication of the received CMT signal with $F(\beta t - l\Delta f)$ and $e^{j2\pi[\beta nT]t}$ which is followed by an integrater and a decision circuit. In the demodulator, where the perfect synchronization of frequency and phase, and the condition of "$\Delta fT$ = integer" are assumed. The latter condition is desirable to make the configuration of the receiver simple. Under the condition of "$\Delta fT \neq$ integer," the carrier phase in $S_{ln}(t)$ (Eq. (25)) changes according to the channel number $l$, therefore the receiver needs to control the phase of multiplying carriers according to the value of $l$.

Furthermore, when the proposed receiver is applied to the case of asynchronous symbol timing between channels, both of the phase and the frequency of the multiplying carriers have to be changed according to the channel number $l$.

The decision sample of the demodulated $n$-th symbol of the $l$-th channel, $Q_{ln}$, is written by

$$\begin{aligned} Q_{ln} &= \int_{t_{la}}^{t_{lb}} v_0(t) S'_{ln}(t) dt \\ &= \int_{t_{la}}^{t_{lb}} \left[ S_{ln}(t) e^{j\theta_{ln}} \right] S'_{ln}(t) dt \end{aligned}$$

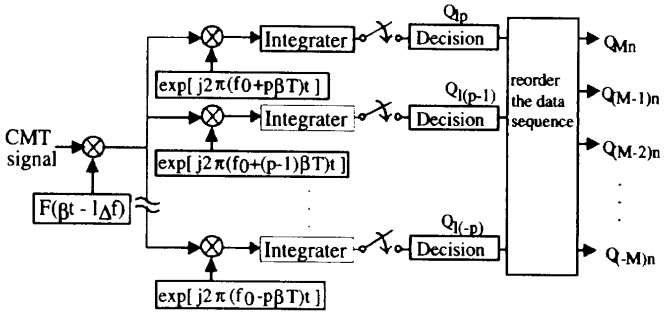


**Fig. 7** Configuration of suboptimal correlation receiver.

$$+\sum_{\substack{k=-M\\k\neq n}}^{M}\sum_{\substack{s=-p\\s\neq n}}^{p}\int_{t_{la}}^{t_{lb}}\left[S_{ks}(t)e^{j\theta_{ks}}\right]S'_{ln}(t)dt \quad (28)$$

$$S'_{ln}(t)=F[\beta(t-T_c)-l\Delta f]e^{j2\pi[\beta(t-T_c)]nT} \quad (29)$$

$$t_{la}=T_c+\frac{1}{\beta}(l\Delta f-\frac{B}{2}) \quad (30)$$

$$t_{lb}=T_c+\frac{1}{\beta}(l\Delta f+\frac{B}{2}) \quad (31)$$

The first term of Eq. (28) represents the desired signal and the second term represents ICI and ISI. Consequently when we demodulate the $n$-th symbol of the $l$-th channel, the signal-to-ICI power ratio (S/ICI) and signal-to-ISI power ratio (S/ISI) are derived as

$$\left(\frac{S}{ICI}\right)_{ln}=\frac{\left(Re\left[\int_{t_{la}}^{t_{lb}}S_{ln}(t)S'_{ln}(t)dt\right]\right)^2}{\left(\sum_{\substack{k=-M\\k\neq l}}^{M}Re\left[\int_{t_{la}}^{t_{lb}}S_{kn}(t)S'_{ln}(t)dt\right]\right)^2} \quad (32)$$

$$\left(\frac{S}{ISI}\right)_{ln}=\frac{\left(Re\left[\int_{t_{la}}^{t_{lb}}S_{ln}(t)S'_{ln}(t)dt\right]\right)^2}{\left(\sum_{\substack{s=-p\\s\neq n}}^{p}Re\left[\int_{t_{la}}^{t_{lb}}S_{ls}(t)S'_{ln}(t)dt\right]\right)^2} \quad (33)$$

Figures 8 and 9 show the S/ICI and the S/ISI performances of the center channel versus chirping dispersion time normalized by symbol duration ($T_c/T$). The total number of channels, $2M+1$, is 3, and the roll-off index $\alpha$ and the symbol number $n$ are parameters. In the figures, $n=p$ indicates the highest frequency symbol in the CMT signal.

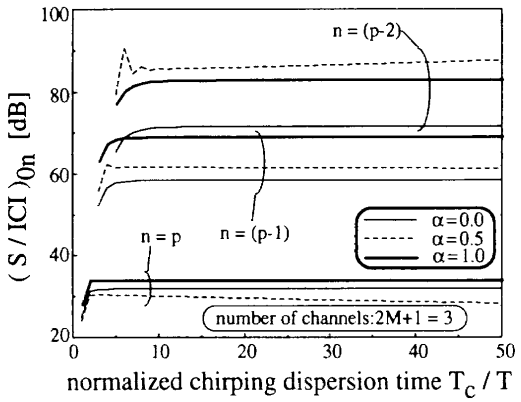


**Fig. 8** S/ICI versus chirping dispersion time.

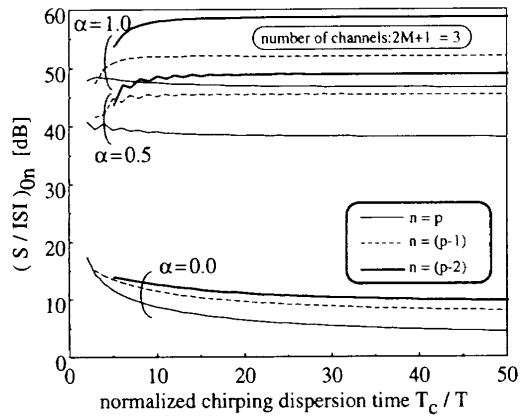


**Fig. 9** S/ISI versus chirping dispersion time.

As described in Sect. 3, the convolution of $G(\beta t)$ with $F(\beta t)$ causes spreading sidelobes of each channel's pulse, therefore the ICI. Figure 8 shows the most highest frequency symbol is most degraded and its S/ICI doesn't change even if the $T_c$ becomes large, though the S/ICI of the center frequency symbol or the identical frequency symbol increases. The reason is that the larger spreading of sidelobe in the time domain is caused by the larger truncation of originally spreading sidelobe in the frequency domain, and the highest frequency symbol in the CMT signal suffers from the largest truncation (see Fig. 5).

On the other hand, it is seen from Fig. 9 that the difference of the roll-off index influences the S/ISI more than that of the symbol number, and $\alpha=1$ gives the maximum S/ISI. The reason is that the spreading of each symbol's spectrum shape in the CMT signal becomes narrowest when $\alpha=1$, and it results in the smallest truncation part and distortion.

## 5. The Double CMT System

As shown in Sect. 4, the S/ICI and the S/ISI performances of the highest and the lowest frequency symbol in the CMT signal are most degraded and dominate the total system performance. Figure 8 shows that there exists 34 [dB] difference between the S/ICI of $n=p$ and that of $n=p-1$ when $T_c/T=5.0$ and $\alpha=1.0$.

Similar problem occurs in the Group Demodulation system using Chirp Fourier transform for FDM signals. To solve this problem, the dual-parallel use of Chirp Fourier transform has been proposed in [12]. In the system, the chirp sweep timings of the two transformers are offset by half of the chirping dispersion time from each other, and only the center $k/2$ symbols ($k=T_c/T$) from each transformer output is used for demodulation.

The parallel use of Chirp Fourier transformer is also effective for our system, and we call the system "Double CMT system." However, we have to transfer the two output signals from CMTs through analog optic-fiber link simultaneously and demodulate the transformed signal at the CS. One solution is to prepare two independent optic-links to transfer the two parallel outputs from CMTs, but it increases the complexity of network configuration. So we propose to multiplex the two parallel outputs into a single optic-fiber link with TDM format. Figures 10 illustrates the configuration of the double CMT system. It consists of two CMT whose chirp sweep timings are offset from each other by half of the chirping dispersion time, $T_c/2$, in the case of "$T_c/T$ = even integer," otherwise by $(T_c+T)/2$ in the

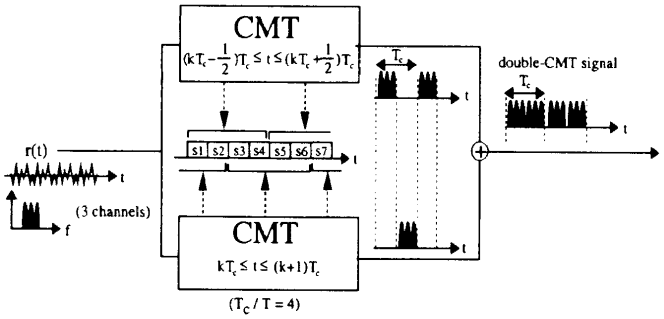


**Fig. 10** Configuration of double CMT.

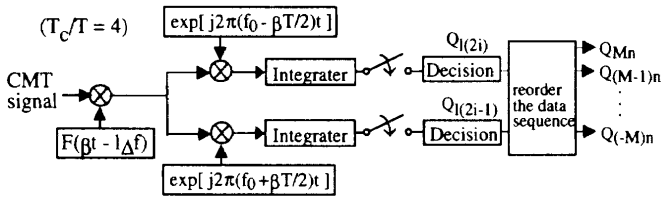


**Fig. 11** Configuration of the receiver for double CMT system.

case of "$T_c/T$ = odd integer." Equation (19) shows that when we enlarge the frequency range of sweep, $\Delta F$, into more than double of total radio bandwidth $B_{total}$, we can reduce the time width of the TLFT signal, $U^{(k)}(t) \cdot g(t-(k+1)T_c)$, to less than $T_c/2$. Consequently two CMT outputs are time-division-multiplexed by simply adding the two outputs.

Figure 11 illustrates the configuration of the receiver for the double CMT system in the case of $T_c/T = 4.0$. At the receiver, we use only center $T_c/2T$ symbols in the frequency domain to demodulate and it is sufficient to prepare only $T_c/(2T)$ demodulation circuits in the case of "$T_c/T$ = even integer." The sampling process is executed at the interval of the half of $\Delta f/\beta$ and the demultiplexing for two parallel CMT outputs is not required. In the case of "$T_c/T$ = odd integer," we need $(T_c+T)/(2T)$ demodulation circuits.

Another important merit of the double CMT system is a robustness against the imperfect synchronization between the chirping dispersion time period and the symbol duration assumed in Sect. 4. The imperfection generates more truncated part and performance degradation mainly to the highest or the lowest frequency symbol in the CMT signal. However the double CMT system doesn't use the damaged symbol for demodulation.

## 6. Theoretical Analysis of SNR and Overall Performance

In this section, we theoretically analyze the signal-to-noise power ratio (SNR) at the suboptimal correlation detection in the CMT/IM/DD system. Here assuming the $T_c$ is enough larger than $T$, we neglect the effect of the convolution with $G(\beta t)$ in Eq. (24). The suboptimal correlation detection becomes the optimum detection scheme which maximizes the SNR because the signal for correlation at the receiver is matched to the waveform of received signal.

Expressing the non-linearity of LD by use of polynomial equation [14], the optical intensity $P(t)$ from the LD modulated by the CMT signal is given by

$$P(t) = P_0[1 + mV(t) + a_2\{mV(t)\}^2 + a_3\{mV(t)\}^3 + \cdots] \quad (34)$$

where $P_0$ is the average transmitting optical power and $m$ is the modulation index. When this optical signal is received at the CS, the output current of photo-diode (PD), $I_o(t)$, is given by

$$I_o(t) = \alpha_o P_r(1 + mV(t)) + I_{RIN}(t) + I_{shot}(t) + I_{th}(t) + I_{im3}(t) \quad (35)$$

where $P_r$ and $\alpha_o$ are the average received optical power and the responsibity of PD, respectively. $I_{RIN}(t)$, $I_{shot}(t)$, and $I_{th}(t)$ are the relative intensity noise current, the shot noise current, and the thermal noise current, respectively. $I_{im3}(t)$ is the 3rd order intermodulation distortion current. Assuming each noise current is white noise current, the power spectrum density (PSD) level of each noise current is given by

$$n_{RIN} = RIN(\alpha_o P_r)^2 \quad (36)$$

$$n_{shot} = 2e\alpha_o P_r \quad (37)$$

$$n_{th} = \frac{4k_B T_{th}}{R} \quad (38)$$

where $RIN$, $k_B$, $T_{th}$ and $R$ are the PSD of relative intensity noise of LD, Boltzmann constant, the noise temperature, and the load resistance, respectively. In the case of the $N$ unmodulated carriers with equal amplitude and equal frequency spacing, the IM3 power in the $k$-th carrier band, $< I_{im3}^2 >_{(N,k)}$, is given by [5], [15]

$$< I_{im3}^2 >_{(N,k)} = \begin{cases} \frac{1}{2}\left(\frac{3}{4}a_3 m^3 D_{(N,k)}^{(2)} + \frac{3}{2}a_3 m^3 D_{(N,k)}^{(3)}\right)^2 (\alpha_o P_r)^2 & (N \geqq 3) \\ 0 & (N < 3) \end{cases} \quad (39)$$

$$D_{(N,k)}^{(2)} = \frac{1}{2}[N - 2 - \frac{1}{2}\{1-(-1)^N\}(-1)^k] \quad (40)$$

$$D_{(N,k)}^{(3)} = \frac{k}{2}(N-k+1) + \frac{1}{4}\{(N-3)^2 - 5\} - \frac{1}{8}\{1-(-1)^N\}(-1)^{N+k} \quad (41)$$

The $< I_{im3}^2 >_{(N,k)}$ has the largest value at the center carrier frequency band. We assume that the IM3 current in the CMT system is the bandlimited white noise current with its PSD level of $n_{im3}$.

$$n_{im3} = \begin{cases} \frac{(2p+1)\cdot < I_{im3}^2 >_{(2p+1,p)}}{\Delta F} & (2p+1 \geqq 3) \\ 0 & (2p+1 < 3) \end{cases} \quad (42)$$

where $2p+1$ is the number of carriers represented by $2p+1 = T_c/T$.

The symbol energy $E_s$ is written by

$$E_s = \frac{1}{2}(\alpha_o P_r)^2 m^2 \int_{-\infty}^{\infty} F^2(\beta t)dt = \frac{1}{2}(\alpha_o P_r)^2 m^2 \frac{T_c}{T\Delta F} \quad (43)$$

where the modulation index $m$ needs to satisfy the following condition in order not to cause the over modulation distortion at LD in Eq. (34).

$$m \leqq \frac{1}{2p+1} = \frac{T}{T_c} \quad (44)$$

It is seen from Eqs. (43) and (44) that the symbol energy $E_s$ decreases as $\Delta F$ increases because the pulse waveform of the CMT signal becomes narrower, and that $E_s$ also decreases as $T_c$ becomes large because the number of carriers, that is, $T_c/T$ increases and $m$ should be proportional to the inverse of it.

The SNR at a sampling time of the correlation detection, that is, the energy contrast, is given by,

$$\left(\frac{S}{N}\right)_{cmt} = \frac{E_s}{n_{RIN} + n_{shot} + n_{th} + n_{im3}} \quad (45)$$

There exists the optimum modulation index $m_{opt}$ which gives the maximum SNR because $n_{RIN}$, $n_{shot}$ and $n_{th}$ are independent to the modulation index $m$, while $E_s$ increases proportional to $m^2$, and $n_{im3}$ increases proportional to $m^6$. The $m_{opt}$ is given by

$$m_{opt} = \left(\frac{n_{RIN} + n_{shot} + n_{th}}{2n_{im3}|_{m=1}}\right)^{\frac{1}{6}} \quad (46)$$

where $m_{opt}$ needs to satisfy the condition of Eq. (44). Regarding the frequency range of sweep, $\Delta F$, we can choose value of $\Delta F$ more than $B_{total}$ (Eq. (20)), but since $E_s$ is proportional to the inverse of $\Delta F$, it should be the following value:

$$\Delta F = \begin{cases} B_{total} & \text{(single CMT)} \\ 2B_{total} & \text{(double CMT)} \end{cases} \quad (47)$$

Figure 12 shows the $(S/N)_{cmt}$ versus the number of FDM radio channels for both the single CMT scheme and the double CMT scheme, and for different values of the normalized chirping dispersion time, $T_c/T$. In the calculation, the optimum modulation index $m_{opt}$ and parameters shown in Table 1 are used.

It is seen from the Fig. 12 that the SNR decreases as the number of channels increases and that the SNR of the double CMT is degraded than the that of the single CMT scheme because the increase of the frequency range of sweep, $\Delta F$, causes the decrease of the symbol energy. It is also seen that the SNR for large $T_c/T$ is degraded because of the increase of the intermodulation distortion power, so it is desired to use small $T_c/T$. In

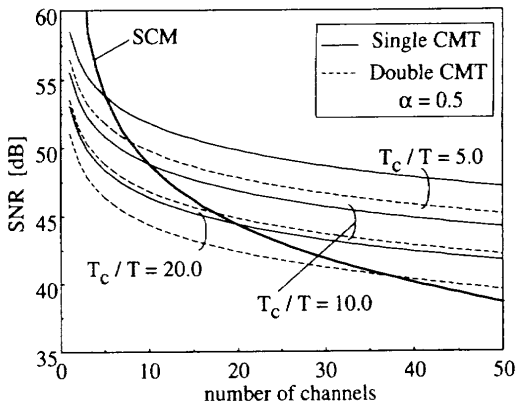


**Fig. 12** SNR versus the number of channels.

**Table 1** Parameters used in calculation.

| | | | |
|---|---|---|---|
| $RIN$ | −152[dB/Hz] | $T_{th}$ | 300[K] |
| $\alpha_o$ | 0.8[A/W] | $R$ | 50Ω |
| $a_3$ | 0.01 | $P_r$ | −10[dBm] |
| $1/T$ | 192 symbol/s | $\Delta f$ | 2/T |

the figure, the SNR performance of the conventional SCM scheme is also shown. It is seen that the SNR of the SCM system more rapidly decreases compared to the proposed system as the number of channels increases because of the increase of the intermodulation distortion power. As a result, the SNR performance of the proposed system becomes superior to the SCM system in the condition of large number of channels in spite of the value $T_c/T$. In the case of $T_c/T = 5.0$, the SNR of the single CMT system is superior at the number of channels more than 6, and that of the double CMT system is superior at the number of channels more than 8.

Figure 13 shows the overall SNR performance of the proposed system considering the S/ICI, the S/ISI and the SNR, which is given by

$$\left(\frac{S}{N+I}\right) = \left[\left(\frac{S}{ICI}\right)^{-1} + \left(\frac{S}{ISI}\right)^{-1} + \left(\frac{S}{N}\right)^{-1}\right]^{-1} \quad (48)$$

In the calculation of the (S/ICI) and the (S/ISI), $\alpha = 0.5$ is assumed, and we examine the performances of the most degraded symbol, that is, the highest frequency symbol in the CMT signal. It is seen from the figure that the overall performance of the single CMT system is inferior to the SCM system in spite of value $T_c/T$ because it is dominated by the low S/ICI performance. On the other hand, the double CMT system can much improve the overall performance because it is dominated by the SNR performance shown in Fig. 12, and it is superior to the SCM system at $T_c/T = 5.0$ and the number of radio channels more than 26. In the figure, 3[dB] improvement of the overall performance is obtained when the number of channels is 50 and $T_c/T = 5.0$. This superiority is caused by the fact the CMT system can

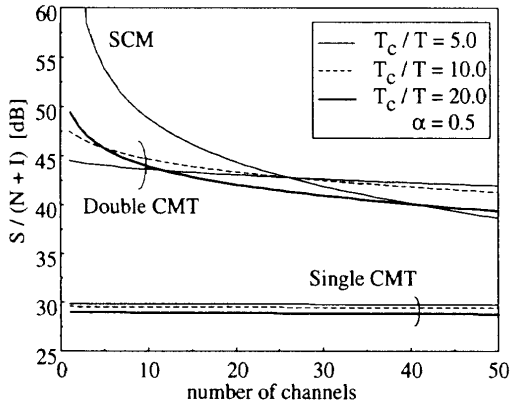


**Fig. 13** S/(N+I) versus the number of channels.

decrease the number of carriers and is tolerable against the LD nonlinearity. Consequently, the performance of the CMT system is superior to the SCM system in the condition that the LD nonlinearity dominates the signal performance.

## 7. Conclusion

In this paper, we proposed the CMT/IM/DD system suitable for Radio High-way Networks in the point of seamless routing of radio signals, and theoretically analyzed the SNR performance on up-link considering the ICI, the ISI, the LD nonlinearity, and the receiver noise inherent to the IM/DD system. Furthermore for decreasing the ICI and the ISI, we newly proposed the double CMT system. We discussed the relationship between the signal performance and the parameters inherent to the CMT/IM/DD system and further discussed it compared to the conventional SCM system. Following results are obtained.

1. We can successfully transform FDM multiple radio services into TDM format signals by using CMT. Then the CMT/IM/DD system can construct more simple and seamless Radio Highway Networks because the distinction and the routing of each radio service in the networks are easily realized in the optical domain using simple photonic time switch.

2. Using the suboptimal correlation demodulator, we can directly demodulate the received CMT signal with high (S/ISI) and high (S/ICI), however the performances are different according to the symbol number and the roll-off index of pulse shaping. In particular, the S/ICI performance of the highest and the lowest frequency symbol in the CMT signal is most degraded, and using largest value of roll-off index can most improve the S/ISI performance.

3. The double CMT system can much improve the S/ICI and the S/ISI performance though the SNR performance is degraded. The double CMT system obtains 32[dB] improvement of the S/ICI in the case of $T_c/T = 5.0$ and $\alpha = 1.0$.

4. The SNR performance of the CMT/IM/DD system is superior to the SCM link in spite of the value $T_c/T$ when the number of radio channels becomes large.

5. The overall SNR performance of the CMT/IM/DD system is superior to the SCM link when the number of channels is large and the double CMT is used. In the case that the number of channels is 50, $T_c/T = 5.0$, and $\alpha = 0.5$, we obtain 3[dB] improvement of the overall performance.

## Acknowledgments

This paper is partially supported by the Grant-in-Aid for General Scientific Research(B) No.09450154, from the Ministry of Education, Science Research and Culture.

### References

[1] S. Komaki, K. Tsukamoto, M. Okada, and H. Harada, "Proposal of radio high-way networks for future multimedia-personal wireless communications," 1994 IEEE International Conference on Personal Wireless Communications (ICPWC 94'), Bangalore India, pp.204–208, Aug. 1994.

[2] H. Harada, K. Tsukamoto, S. Komaki, and N. Morinaga, "Optical TDM scheme for fiber-optic millimeter-wave radio system," IEICE Trans. Commun., vol.J77-CI, no.11, pp.1–10, Nov. 1994.

[3] H. Harada, S. Kajiya, K. Tsukamoto, S. Komaki, and N. Morinaga, "TDM intercell connection fiber-optic bus link for personal radio communication system," IEICE Trans. Commun., vol.E78-B, no.9, pp.1287–1294, Sept. 1995.

[4] Y. Shoji, K. Tsukamoto, and S. Komaki, "Proposal of the radio high-way networks using asynchronous time division multiple access," IEICE Trans. Commun., vol.E79-B, no.3, pp.308–315, March 1996.

[5] H. Mizuguti, T. Okuno, S. Komaki, and N. Morinaga, "Performance analysis of optical fiber link for microcellular mobil communication systems," IEICE Trans. Electron., vol.E76-C, no.2, pp.271–278, Feb. 1993.

[6] A.J. Mervyn, P.M. Grand, and J.H. Collins, "The theory, design, and applications of surface acoustic wave Fourier-transform processors," Proc. IEEE, vol.68, no.4, pp.450–468, April 1980.

[7] W.L. Ha, R.M. Fortenberry, and R.S. Tucker, "Demonstration of photonic fast packet switching at 700 Mbit/s data rate," Electron. Lett., vol.27, no.10, pp.789–790, May 1991.

[8] F. Takahata, M. Yasunaga, and Y. Hirata, "A PSK group modem based on digital signal processing: Algorithm, hardware design, implementation and performance," International Journal of Satellite Communications, vol.6, pp.253–266, 1988.

[9] K.Y. Eng and O.-C. Yue, "Time compression multiplexing of multiple television signals in satellite channels using chirp transform processors," IEE Trans. Commun.,

vol.COM-29, no.12, pp.1832–1840, Dec. 1981.
[10] T. Kohri, M. Morikura, and S. Kato, "Non-regenerative onboard FDM/TDM transmultiplexer," IEICE Trans., vol.J69-B, no.11, pp.1480–1487, Nov. 1986.
[11] K. Kobayashi, T. Kumagai, and S. Kato, "A group demodulator employing multi-symbol chirp Fourier transform," IEICE Trans. Commun., vol.E77-B, no.7, pp.905–910, July 1994.
[12] T. Kumagai and K. Kobayashi, "A new group demodulator with multi-symbol chirp Fourier transform for mobile communication systems," Proc. IEEE ICUPC'95, pp.397–401, Nov. 1995.
[13] K. Ohno and F. Adachi, "Postdetection diversity reception of QDPSK signals in land mobile radio channels," IEICE Trans., vol.J73-B-II, no.11, pp.651–657, Nov. 1990.
[14] C.J. Daly, "Fiber optic intermodulation distortion," IEEE Trans. Commun., vol.COM-38, no.8, pp.1954–1958, Aug. 1982.
[15] R.J. Westcott, "Investigation of multiple f.m./f.d.m. carriers through a satellite t.w.t. operating near to saturation," Proc. IEE, vol.114, no.6 pp.726–740, June 1967.

## Appendix

In this section, we prove the orthogonality of $S'_{ln}(t) = F[\beta t - l\Delta f]e^{-j2\pi[\beta t - l\Delta f]nT}$ where $G(\beta t)$ is removed from $S_{ln}(t)$ in Eq. (25). Generally for the two waveforms, $\psi_i(t)$ and $\psi_k(t)$, to be orthogonal, they must fulfill the orthogonality constraint of the Equation,

$$\int_{-\frac{T_s}{2}}^{\frac{T_s}{2}} \psi_i(t)\psi_k(t)dt = K_i\delta_{ik} \quad (i,\ k : \text{integer}) \quad (A\cdot 1)$$

$$\delta_{ik} = \begin{cases} 1 & (i = k) \\ 0 & (\text{otherwise}) \end{cases} \quad (A\cdot 2)$$

where $T_s$ and $K_i$ are the symbol duration and constants respectively. The orthogonality of $S'_{ln}(t)$ among different $l$ is obviously satisfied because $F(f)$ is bandlimited. Then, we investigate the following complex correlation function $R_{ik}$ to investigate the orthogonality among different $n$.

$$\begin{aligned} R_{ik} &= \int_{-\frac{B}{2\beta}}^{\frac{B}{2\beta}} S'_{0i}(t)\{S'_{0k}(t)\}^* dt \\ &= \int_{-\frac{B}{2\beta}}^{\frac{B}{2\beta}} |F[\beta t]|^2 e^{-j(2\pi d_{ik}\beta t + \theta_{ik})} dt \end{aligned} \quad (A\cdot 3)$$

where, $d_{ik} = i - k$ and $\theta_{ik} = \theta_i - \theta_k$. The real part of $R_{ik}$ is given by

$$\begin{aligned} Re[R_{ik}] = &\int_{-\frac{B}{2\beta}}^{\frac{B}{2\beta}} |F[\beta t]|^2 \cos[2\pi d_{ik}\beta t]dt \cdot \cos[\theta_{ik}] \\ &+ \int_{-\frac{B}{2\beta}}^{\frac{B}{2\beta}} |F[\beta t]|^2 \sin[2\pi d_{ik}\beta t]dt \cdot \sin[\theta_{ik}] \end{aligned} \quad (A\cdot 4)$$

Because of the integration of the odd function $F[f]$ given by Eq. (26), the second term in Eq. (A·4) comes to be zero. Then $Re[R_{ik}]$ can be calculated as

$$\begin{aligned} &Re[R_{ik}] \\ &= 2\int_0^{\frac{1-\alpha}{2T}} \cos(2\pi T d_{ik} f)df \\ &\quad + 2\int_{\frac{1-\alpha}{2T}}^{\frac{1+\alpha}{2T}} \cos(2\pi T d_{ik} f) \\ &\quad \times \cos^2\left[\frac{\pi T}{2\alpha}\left(t - \frac{1-\alpha}{2T}\right)\right] dt \\ &= \begin{cases} \frac{1}{T} & (d_{ik} = 0) \\ 0 & (\text{otherwise}) \end{cases} \end{aligned} \quad (A\cdot 5)$$

Consequently, we have proved that $S'_{ln}(t)$ is an orthogonal signal set.

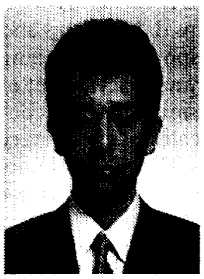

**Yozo Shoji** was born in Kanagawa, Japan, on August 15, 1972. He received the B.E. and M.E. degrees in Electrical Engineering from Osaka University, Osaka, Japan, in 1995 and 1996 respectively. He is currently pursuing the Ph.D. degree at Osaka University. He is engaging in the research on radio and optical communication systems.

**Katsutoshi Tsukamoto** was born in Shiga, Japan in October 7, 1959. He received the B.E., M.E. and Ph.D. degrees in Communication Engineering from Osaka University, in 1982, 1984 and 1995 respectively. He is currently a Associate Professor in the Department of Communications Engineering at Osaka University, engaging in the research on radio and optical communication systems. He is a member of IEEE.

**Shozo Komaki** was born in Osaka, Japan, in 1947. He received B.E., M.E. and Ph.D. degrees in Electrical Communication Engineering from Osaka University, in 1970, 1972 and 1983 respectively. In 1972, he joined the NTT Radio Communication Labs., where he was engaged in repeater development for a 20-GHz digital radio system, 16-QAM and 256-QAM systems. From 1990, he moved to Osaka University, Faculty of Engineering, and engaging in the research on radio and optical communication systems. He is currently a Professor of Osaka University. Dr. Komaki is a senior member of IEEE, and a member of the Institute of Television Engineers of Japan (ITE). He was awarded the Paper Award and the Achievement Award of IEICE, Japan in 1977 and 1994 respectively.